

Raman scattering near a quantum critical point

J.K. Freericks* and T.P. Devereaux†

**Department of Physics, Georgetown University, Washington, DC 20057, U.S.A.*

†*Department of Physics, University of Waterloo, Canada*

(October 31, 2018)

Electronic Raman scattering experiments in a wide variety of materials (ranging from mixed-valence materials to Kondo insulators to high-temperature superconductors) show anomalous behavior in the B_{1g} channel when the system is on the insulating side of the metal-insulator transition. Here we provide an exact solution for B_{1g} Raman scattering in the Falicov-Kimball model, show how these theoretical results are universal near the metal-insulator transition and show how they produce the two main features seen in experiments near a quantum critical point: (i) the rapid appearance of low-energy spectral weight as T is increased from 0 and (ii) the existence of an isosbestic point (where the Raman response is independent of T at a characteristic frequency).

Raman scattering has long been applied to study metals, insulators, semiconductors, and superconductors. Via light's coupling to the electron's charge, inelastic light scattering can reveal electron dynamics over a wide range of energy scales and temperatures. More recently, Raman scattering has played a strong role in elucidating the nature of electron dynamics in the high temperature superconductors over the entire region of their phase diagram. These studies have been particularly useful in shedding light on superconducting and pseudogap energies and on magnon scales and dispersions. Systems as disparate as mixed-valence compounds (such as SmB_6 [1]), Kondo-insulators (such as FeSi [2]), and the underdoped cuprate high temperature superconductors [3–5]), show temperature-dependent B_{1g} Raman spectra that are both remarkably similar and quite anomalous, suggesting a common mechanism governing transport. As these materials are cooled, a pile up of spectral weight appears for moderate photon energy losses with a simultaneous reduction of the low frequency spectral weight. This spectral weight transfer is slow at high temperatures and then rapidly increases as temperature is lowered towards a putative quantum critical point (corresponding to a metal-insulator transition). In addition, the spectral range is divided into two regions: one where the Raman response decreases as T is lowered and one where the response increases. These regions are separated by a so-called isosbestic point, which is defined to be the characteristic frequency where the Raman response is independent of temperature.

While the existence of anomalous features in Raman scattering near a quantum critical point has been seen for some time, there is no theoretical understanding that connects the metallic and insulating states. In 1991, Shraiman and Shastry [6] outlined a procedure to construct a theory that can interpolate from a metal to an insulator. However, due to the ever increasing Hilbert space needed to describe a metal from the insulating side, or the lack of a clear picture of quasiparticles from the metallic side, quantitative calculations were not feasible. One is then left with approximate methods (such as per-

turbation theory for the Hubbard model) or more phenomenological approaches to construct a Raman theory which suffer the limitations of being unable to reach different phases and of lacking a microscopic basis.

Here we provide the first exact theoretical description of Raman scattering near a quantum metal-insulator transition that contains all of the anomalous behavior seen in experiments on these strongly correlated materials. We choose the spinless Falicov-Kimball model [7] as our canonical model for Raman scattering. It contains two types of electrons: itinerant band electrons and localized (d or f) electrons. The band electrons can hop between nearest neighbors [with hopping integral $t^*/(2\sqrt{d})$ on a d -dimensional cubic lattice], and they interact via a screened Coulomb interaction with the localized electrons (that is described by an interaction strength U between electrons that are located at the same lattice site). We measure all energies in units of t^* . The Hamiltonian is

$$H = -\frac{t^*}{2\sqrt{d}} \sum_{\langle i,j \rangle} d_i^\dagger d_j + E_f \sum_i w_i - \mu \sum_i (d_i^\dagger d_i + w_i) + U \sum_i d_i^\dagger d_i w_i, \quad (1)$$

where d_i^\dagger (d_i) is the spinless conduction electron creation (annihilation) operator at lattice site i and $w_i = 0$ or 1 is a classical variable corresponding to the localized f -electron number at site i . We will adjust both E_f and μ so that the average filling of the d -electrons is $1/2$ and the average filling of the f -electrons is $1/2$ ($\mu = U/2$ and $E_f = 0$).

The Raman response is found from the frequency-dependent density-density correlation function that is depicted in Figure 1. The Raman scattering process involves a two-photon-electron-hole vertex function that is called the Raman scattering amplitude $\gamma(\mathbf{k})$. In addition to the effects of the Raman scattering amplitude, the density-density correlation function is, in general, also renormalized by the irreducible dynamical charge vertex, which is denoted by Γ in Figure 1. Evaluating the di-

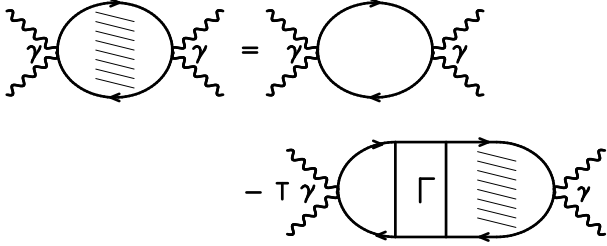


FIG. 1. Dyson equation for the nonresonant Raman response function. Solid lines denote electron propagators and wavy lines denote photon propagators. The shading denotes the fully renormalized susceptibility and the symbol Γ is the irreducible frequency-dependent charge vertex.

agrams in the standard fashion produces the following result:

$$\chi(i\nu_l) = \sum_{\mathbf{k}} \int_0^\beta d\tau e^{i\nu_l \tau} \quad (2)$$

$$\times \left\{ \frac{\text{Tr} T_\tau \langle e^{-\beta H} \rho_{\mathbf{k}}(\tau) \rho_{\mathbf{k}}(0) \rangle}{Z} - \left[\frac{\text{Tr} \langle e^{-\beta H} \rho_{\mathbf{k}}(0) \rangle}{Z} \right]^2 \right\},$$

with the uniform ($\mathbf{q} = 0$) Raman density operator

$$\rho_{\mathbf{k}} = \gamma(\mathbf{k}) d_{\mathbf{k}}^\dagger d_{\mathbf{k}}, \quad d_{\mathbf{k}} = \frac{1}{N} \sum_j e^{-\mathbf{R}_j \cdot \mathbf{k}} d_j, \quad (3)$$

$Z = \text{Tr} \langle e^{-\beta H} \rangle$, the partition function, and $i\nu_l = 2i\pi l T$ the bosonic Matsubara frequency (the τ -dependence of the operators is with respect to the full Hamiltonian). The Raman scattering amplitude $\gamma(\mathbf{k})$ is a complicated function of the incoming and outgoing photon polarizations, of the photon energies, and the polarizability of the medium. In nonresonant Raman scattering one neglects the frequency dependence of the Raman scattering amplitude, and characterizes the Raman response in terms of the different spatial symmetries of the remaining function $\gamma(\mathbf{k})$. One can expand this function in a Fourier series and examine the contributions of the lowest components of the series, and compare them to experiment (the lowest order B_{1g} contribution is $\gamma(\mathbf{k}) = \sum_{j=1}^d (-1)^j \cos \mathbf{k}_j$, with $d \rightarrow \infty$ the spatial dimension). More sophisticated approaches would calculate the Raman scattering amplitude from “first-principles” and would include any possible resonant Raman scattering effects. We leave those pursuits to future work.

The Falicov-Kimball model can be solved exactly in the infinite-dimensional limit by using dynamical mean-field theory (see Ref. [8] for details). The dynamical charge vertex is local in infinite dimensions which implies that correlation functions that have the same symmetry as the lattice are renormalized due to this charge vertex, but correlation functions that are orthogonal to the lattice, have no vertex corrections, and so they are represented by their bare bubble diagrams [9]. Although the

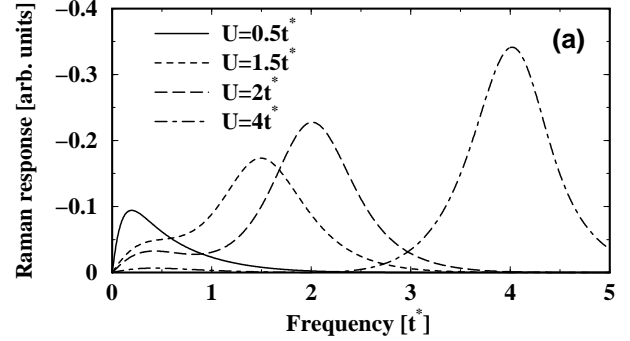


FIG. 2. B_{1g} Raman response as a function of U at $T = 0.5$.

fully symmetric A_{1g} Raman response can be calculated directly, we concentrate here on the B_{1g} response, which is described by the bare bubble diagram in Figure 1. In this case, a straightforward symmetry analysis also shows that resonant Raman scattering effects vanish for nearest neighbor hopping on a hypercubic lattice in large dimensions, so the total Raman response is represented by these nonresonant results.

The Falicov-Kimball model has a ground state that is not a Fermi liquid because the lifetime of a quasiparticle is finite at the Fermi energy. As U increases, the system first enters a pseudogap phase, where spectral weight is depleted near the chemical potential, and then undergoes a metal-insulator transition. The interacting density of states (DOS) is, however, temperature-independent for fixed U and fixed electron fillings. For half-filling, $U < 0.65$ corresponds to a weakly-correlated metal, while a pseudogap phase appears for $0.65 < U < 1.5$ moving through a quantum critical point at $U = 1.5$ to the insulator phase $U > 1.5$ (we neglect all possible charge-density-wave phases here).

The Raman response is calculated in a similar fashion to the dynamical charge susceptibility [11]: the Dyson equation of Figure 1 is formally analytically continued to the real axis, where the expression for the Raman response is found to depend solely on complex integrals of the interacting single-particle DOS. In Figure 2 we plot the Raman response at a fixed temperature $T = 0.5$ for different values of U . For small values of U , a small scattering intensity is observed due to the weak interaction among “quasiparticles” providing a small region of phase space allowable for pair scattering. The peak of the response reflects the dominant energy scale for scattering, as is well known in metals [12] and the high-energy tail is the cutoff determined by the finite energy band. As U increases, the low-frequency response is depleted as spectral weight gets shifted into a large charge transfer peak at a frequency $\sim U$. The charge transfer peak begins to appear for values of U for which the DOS is still finite at the Fermi level and becomes large in this pseu-

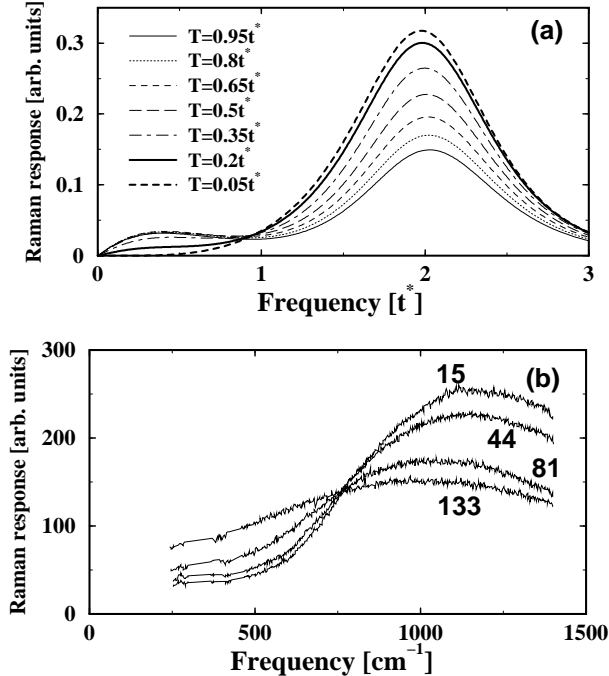


FIG. 3. B_{1g} (a) Theoretical Raman response as a function of temperature for $U = 2$ (which lies just on the insulating side of the metal-insulator transition) and (b) experimental [2] Raman response for FeSi at moderate to low temperatures (where the isosbestic point and low temperature spectral weight depletion is seen). The experimental graphs are labeled by the temperature (in K) where the data was collected.

dogap phase before growing even larger in the insulating phase. Notice how low-frequency spectral weight remains even as one is well on the insulating side of the quantum critical point. It is these spectral features that are characteristically seen in the experiments and which can only be seen in a theory that approaches the quantum critical point.

In Figure 3(a) we plot the temperature dependence on the insulating side of the metal-insulator transition. For small values of U the spectra are only slightly dependent on temperature due largely to the small changes in kinetic energy with T . As U increases into the pseudogap and insulating phases, nontrivial temperature dependences begin to appear. The total spectral weight increases dramatically with decreasing temperature as charge transfer processes become more sharply defined. At the same time, the low-frequency response depletes with lowering temperatures, vanishing at a temperature which is on the order of the $T = 0$ insulating gap. This behavior is precisely what is seen in experiment [2] on FeSi at low temperatures 3(b) where both the isosbestic point and the low temperature spectral weight depletion can be seen.

We attribute the presence of a low-frequency response in a system which is a strongly correlated insulator to the appearance of thermally activated transport channels. In the insulating phase at zero temperature, the only available intermediate states created by the light must involve double site occupancy of a conduction and a localized electron, with an energy cost of U . This gives the large charge transfer peak at an energy U . As the temperature is increased, for half filling, double occupancy can occur and as a result light can scatter electrons to hop between adjacent unoccupied states either directly or via virtual double occupancies. The number of electrons which can scatter in this fashion increases with increasing temperature, leading to an increase in the low-frequency spectral weight. The frequency range for this low-frequency Raman response is determined by the lower Hubbard bandwidth, which is typically much larger than the temperature at which these features first appear. If one were to interpret the temperature at which the Raman spectral weight starts to deplete as the transition temperature T_c and the range of frequency over which the weight is depleted as the gap Δ , then one would conclude that near the quantum critical point $2\Delta/k_B T_c \gg 1$. This is because the “ T_c ” is determined by the gap in the single-particle density of states (which approaches zero at the quantum critical point), while the “ Δ ” is determined by the width of the lower Hubbard band (which remains finite at the quantum critical point); hence the ratio can become very large near the quantum critical point.

The spectral weight transfer from low frequencies to the charge transfer peak as a function of temperature can be quantified by separating the Raman response into two regions determined by the isosbestic point and plotting the total low-frequency spectral weight versus temperature (not shown). Choosing $U/2$ as the location of the isosbestic point, we find that the reduction of spectral weight from high to low temperatures is over 50 percent even in the weak pseudogap phase, and decreases by well over three orders of magnitude as U increases into the insulating phase ($U = 4$).

Lastly, we plot the inverse slope of the Raman response in Figure 4(a) as a function of temperature for different values of U and the experimental [3] results on optimal and underdoped copper oxides 4(b). Since the self energy is temperature independent, we might expect a constant Raman slope as a function of temperature, as is the case with disordered noninteracting electrons. However, this is not the case due to the formation of a thermally generated band for scattering. For small values of U , the temperature dependence of the Raman inverse slope is weak due to the temperature independence of the self energy. However, as the single-particle bands begin to separate, the relevance of thermally generated double occupancies becomes more pronounced and the inverse slope becomes temperature dependent at low temperatures. We see that as U increases the low temperature slope increases dramatically due to the depletion of low-frequency spectral weight. In particular, even in the pseudogap phase the

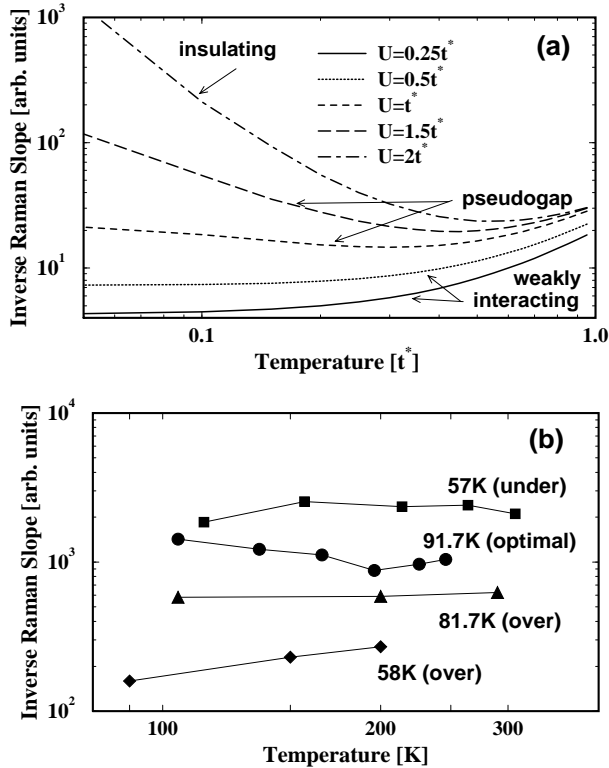


FIG. 4. (a) Theoretical inverse slope of the B_{1g} Raman response and (b) experimental [3] inverse slope for optimal and underdoped high-temperature superconductors (the curves are labeled by their superconducting transition temperature and whether they are under or overdoped; the 57K and 81.7K data have been multiplied by constant factors to separate them).

inverse slope rises with decreasing temperature indicating the proximity to the quantum-critical metal-insulator transition. As U increases into the insulating phase, the temperature dependence of the Raman inverse slope is indicative of the formation of gapped excitations. Note how similar the experimental results are to the theoretical predictions (the lowest temperature data for the underdoped case (top curve) has large error bars because the signal is so small; in all cases as the system becomes underdoped the B_{1g} response behaves more insulator-like).

In more complicated correlated models of the metal-insulator transition the single-particle density of states will have a Fermi liquid peak at low frequencies which may add new features to the Raman response, but on the insulating side of the transition, where most of the anomalous behavior is seen, the single-particle density of states should be very similar to that of the Falicov-Kimball model (except for some additional weak temperature dependence of the interacting DOS), which is why these results are generically expected to be model-independent.

Our theoretical results compare quite favorably to the experimental results seen in a wide range of different materials ranging from mixed-valence compounds [1], to Kondo insulators [2] to the underdoped high-temperature superconducting oxides [3–5]. In particular, all of those experimental systems appear to be close to, but on the insulating side of the metal-insulator transition, and hence they illustrate the two characteristic behaviors seen in our theory: (i) there is a rapid rise in the low-frequency spectral weight at low temperatures (at the expense of the high-frequency spectral weight) and (ii) there is an isosbestic point. Our model always produces an isotropic gap, so we are unable to illustrate some of the behavior seen in the copper-oxides where only the B_{1g} response is anomalous, and the A_{1g} and B_{2g} responses are metallic rather than insulating. But our results do indicate a “universality” and model independence of the Raman response on the insulating side of, but in close proximity to, a quantum critical point. We believe this is the reason why so many different materials show the same generic behavior in their electronic Raman scattering.

ACKNOWLEDGMENTS

J.K.F. acknowledges support of the National Science Foundation under grant DMR-9973225. T.P.D. acknowledges support from the National Research and Engineering Council of Canada. We also acknowledge useful discussions with S.L. Cooper, R. Hackl, J.C. Irwin, M.V. Klein, P. Miller and A. Shvaika. We also thank S.L. Cooper, R. Hackl, and J.C. Irwin for allowing us to reproduce their data.

-
- [1] P. Nyhus *et al.*, Phys. Rev. B **52**, R14308 (1995); *ibid.*, **55**, 12488 (1997).
 - [2] P. Nyhus *et al.*, Phys. Rev. B **51**, R15626 (1995).
 - [3] X. K. Chen *et al.*, Phys. Rev. B **56**, R513 (1997); J. Naeini *et al.*, Phys. Rev. B **59**, 9642 (1999).
 - [4] M. Opel *et al.*, Phys. Rev. B **61**, 9752 (2000).
 - [5] M. Rübhausen *et al.*, Phys. Rev. Lett. **82**, 5349 (1999); S. Sugai and T. Hosokawa, Phys. Rev. Lett. **95**, 1112 (2000).
 - [6] B. S. Shastry and B. I. Shraimann, Int. Journ. Mod. Phys. B **5**, 365 (1991).
 - [7] L. M. Falicov and J. C. Kimball, Phys. Rev. Lett. **22**, 997 (1969).
 - [8] U. Brandt and C. Mielsch, Z. Phys. B **75**, 365 (1989); **79**, 295 (1990); J. K. Freericks, Phys. Rev. B **47**, 9263 (1993).
 - [9] A. Khurana, Phys. Rev. Lett., **64**, 1990 (1990).
 - [10] P.G.J. Van Dongen, and C. Leinung, Ann. Phys. (Leipzig), **6**, 45 (1997).

- [11] A.M. Shvaika, *Physica C* **341-348**, 177 (2000); J.K. Freericks, and P. Miller, *Phys. Rev. B* **62**, 10022 (2000).
- [12] To our knowledge no comprehensive review of electronic Raman scattering in metals exists. General ideas are covered in P. M. Platzmann and N. Tzoar, *Phys. Rev.* **136**, A11 (1964); A. Zawadowski and M. Cardona, *Phys. Rev. B* **42**, 10732 (1990); T. P. Devereaux and A. P. Kampf, **59**, 6411 (1999).